ISSN 1023-1935, Russian Journal of Electrochemistry, 2024, Vol. 60, No. 4, pp. 321–337. © Pleiades Publishing, Ltd., 2024.

Electrochemical Study of the Antitumor Antibiotic Doxorubicin in Its Free Form and Encapsulated in a Biocompatible Copolymer of *N*-Vinylpyrrolidone and (di)Methacrylates[1]

V. A. Kurmaz[a], *, D. V. Konev[a], **, S. V. Kurmaz[a], and N. S. Emel'yanova[a]

[a] *Federal Research Center of Problems of Chemical Physics and Medicinal Chemistry, Russian Academy of Sciences, Chernogolovka, Moscow oblast, Russia*

**e-mail: kurmaz@icp.ac.ru*

***e-mail: dkfrvzh@yandex.ru*

Received June 28, 2023; revised September 18, 2023; accepted October 4, 2023

Abstract—A comparative study of the electrochemical behavior of various forms of the antitumor antibiotic doxorubicin (DOX), both free and encapsulated in micelle-like nanoparticles of the biocompatible amphiphilic copolymer of *N*-vinylpyrrolidone (VP) and methacrylic acid, viz., triethylene glycol dimethacrylate (TEGDM), is carried out in aqueous neutral buffers on a glassy carbon electrode. The hydrodynamic radii R_h of the copolymer and the DOX polymeric nanostructures are determined using dynamic light scattering. Using cyclic and square wave voltammetry, for both forms of DOX at pH 7.24, the two main redox transitions are revealed namely, the irreversible oxidation/rereduction in the potential interval from 0.2 to 0.6 V and the reversible reduction/reoxidation in the interval from –0.4 to –0.7 V (vs. saturated Ag/AgCl), and their redox potentials are determined. For both redox transitions, the potential difference between the corresponding peaks does not exceed several tens (20–30) mV; and, moreover, the oxidation of the encapsulated form proceeds easier as compared with the free form, whereas its reduction is somewhat more difficult. The analysis of the dependence of the reduction current of both DOX forms on the potential scan rate shows that the electron transfer to a free DOX molecule is largely determined by the rate of reagent accumulation in the adsorption layer, whereas the electron transfer to the encapsulated form is characterized by the mixed adsorption-diffusion control. Based on voltammetric data and the results of quantum chemical modeling, it is concluded that a hydrogen bond is formed between the oxygen-containing groups of copolymer's monomeric units and the H atoms in OH and NH_2 groups of DOX. The bond energy in these structures is calculated and shown to be close to the classical values, assuming that the carbonyl group in the VP lactam ring in the encapsulating polymer is the electron donor, and the hydrogen atoms in OH and NH_2 groups of DOX are the electron acceptors. At the same time, the bonds involving oxygen of the ester group in the TEGDM unit are extremely weak.

Keywords: doxorubicin, *N*-vinylpyrrolidone, amphiphilic copolymer, hydrogen bond, adsorption process, adsorption–diffusion process, cyclic voltammetry, square-wave voltammetry, quantum chemical modeling

DOI: 10.1134/S1023193524040050

INTRODUCTION

Quinones pertain to the most popular organic electrochemistry objects and their application field is extremely wide. This class of compounds includes doxorubicin (DOX) which is an efficient antitumor drug with the wide albeit nonselective action field [1]. The detailed mechanism of its effect is sufficiently complicated and yet incompletely clear, and its considerable overall toxicity in combination with the high cardiotoxicity and hipoallergenicity substantially limits its use in therapeutic purposes [2, 3]. However, it is known [4, 5] that DOX can penetrate into DNA, stop its replication, and finally destroy the cancer cell. When penetrated into a living organism, most anticancer drugs actively bind with plasma proteins and red corpuscles, which also lowers the efficiency of drugs and increases their toxicity [4]. This is why the development of methods of making the DOX effect more selective and preventing its noxious aftereffects is a currently topical problem. An important and efficient way of its solution is the encapsulation of the medicinal drugs such as DOX into various structures, both organic/polymeric and inorganic, followed by their targeted delivery to the diseased cells and subsequent liberation in these cells [6]. Hence, the main goals of this method are to lower down the total toxicity of nonselective drugs such as DOX and provide their targeted delivery to the diseased cells with subsequent prolonged liberation.

[1] Published based on the materials of the XX All-Russian Meeting "Electrochemistry of Organic Compounds" (EChOS-2022), Novocherkassk, Russia, October 18–22, 2022.

When considering organic and polymeric carriers, mention should be made of apoferritin [3], i.e., biodegradable polyelectrolyte capsules modified with haematin [7], dextran sulfate and poly-L-arginine [8], the derivatives of cyclodextrin with lipoic acid [9] or nanogels of dextrin [10], synthetic biocompatible polymers and copolymers [11, 12], nanoparticles of polypyrrole and poly(2-ethylamino)ethylmethacrylate [13], etc. The more detailed information can be found in reviews [14, 15]. However, the most popular carrier in this series is polyvinylpyrrolidone (PVP) which is synthesized by polymerization of *N*-vinylpyrrolidone (VP) and exhibits unique physicochemical properties, being chemically inactive, colorless, thermally and pH-stable, well soluble in water, buffers, and organic solvents of different polarity, highly biocompatible and well sorbable [16].

The polymer improves the bioaccessibility of drugs poorly soluble in water and, at the same time, protects them from external factors (oxygen, pH, and temperature). However, PVP as such is insufficiently amphiphilic and does not react to changes in the surrounding pH and temperature, which limits its possibilities as regards the controlled liberation of drugs. To overcome these drawbacks of PVP, it is used in various nanocomposites, e.g., in layered laponite silicate [17], the system DOX-PVP-gold nanoparticles (DOX@PVP-AuNPs) [18] or as the copolymers with widely variable properties that demonstrate wide possibilities in the formation of nanoparticles of various morphology. For instance, the copolymer PVP-*block*-poly(4-vinylpyridine) well dissolves in water and buffers with the wide pH range [4], does not adsorb on the plasma proteins and erythrocytes [4], and can be used as the DOX carrier [11, 14].

The wide prospects are also characteristic of biocompatible copolymers of *N*-vinylpyrrolidone and triethyleneglycol dimethacrylate (TEGDMA), i.e., VP-TEGDMA, and ternary copolymers (terpolymers TP) with methacrylic acid (MAA), viz., VP-MAA-TEGDMA that have branches in side chains [19]. They have the controllable size and molecular mass, are amphiphilic and capable of self-assembling in polar media. The small size of individual macromolecules and their aggregates in water favors their efficient penetration into cells and tissues. On their basis, the nanostructures containing bioactive compounds (BACs) of various nature were synthesized and studied, e.g., metformin—a well-known antidiabetic drug [20], lipophilic organic complexes of platinum(IV) with antitumor activity [21–25], zinc tetraphenylporphyrinate which helps visualization of the intracellular accumulation process [25, 26], the dyes Bengal rose and methylpheophorbide *a* [27, 28], α-tocopherol (E-group vitamin) [29], etc. Furthermore, the high in vitro biocompatibility of these polymeric carriers and their ability to penetrate into cancer cells *HeLa* was demonstrated [30, 31], as well as the ability of the TP-DOX nanostructure to penetrate into normal *Vero* cells [30, 32]. This pointed to the good prospects of the developed materials in the intracellular delivery of BACs.

The copolymers of VP with (di)methacrylates and the BAC nanostructures on their basis [19–30] were characterized by a complex of experimental methods including the transmission and scanning electron microscopy, electron absorption, EPR and NMR spectroscopy, dynamic light scattering (DLS), exclusive chromatography, thermogravimetry, and differential scanning calorimetry. The characterization also included the quantum chemical modeling of BAC–copolymer nanostructures [28, 29, 31] and their electrochemical investigation [21–30]. In particular, using the method of cyclic voltammetry (CVA), it was found that Bengal rose forms a complex with VP-based copolymers, which was confirmed independently by quantum chemical calculations [27, 28]. Earlier, we also showed that the electrochemical properties of some other compounds, namely, zinc tetraphenylporphyrinate [25, 26] and various complexes of Pt(IV) [21–25] can be substantially changed in polymer particles. However, certain problems concerning the energy characteristics of the BAC–copolymer nanostructures, their structure, the binding of BAC with the copolymer, and their similarity and difference from free BAC still remain unclear.

The goal of this study was the comparative investigation of the electrochemical behavior of different doxorubicin forms, i.e., free and encapsulated into the terpolymer VP-MAA-TEGDMA, on the glassy carbon electrode (GCE) and also the quantum chemical analysis of the nature of bonds in the DOX–copolymer structures.

EXPERIMENTAL

We used the terpolymer of *N*-vinylpyrrolidone with triethylene glycol dimethacrylate and methacrylic acid VP–MAA–TEGDMA which was synthesized from the 98 : 2 : 2 mole mixture of monomers in ethanol and characterized in detail in [19, 31]. The pharmaceutic drug doxorubicin hydrochloride (Doxorubicin-Teva, Pharmachemie B.V., Netherlands) contained about 20% of the main substance, lactose monohydrate as the filler (adjuvant), buffer components (Na_2HPO_4, NaH_2PO_4), and inorganic salts (NaCl, KCl) of the special grade of purity which were used without additional cleaning. All solutions were prepared using triply distilled water and controlled during electrochemical experiments (before and after) using a spectrophotometer WPA (UK). The DOX concentration in the pharmaceutical drug was determined by the spectroscopic method using calibration curves and based on the absorption band at 500 nm in the spectra of aqueous solutions of DOX, copolymer, and polymer

compositions; the cuvette thickness was 0.2, 0.5, 1.0, or 2.0 cm.

To prepare the DOX systems based on the terpolymer VP–MAA–TEGDMA, into a terpolymer solution in isopropanol (2 mg/mL) with the volume of 44 mL, we added 2.75 mL DOX solution dropwise on constant stirring by a magnetic stirrer. The DOX content was 3.1 mass % per the terpolymer mass. For removing the solvents, the composite was dried to constant weight in air and under reduced pressure. The polymer composite powder was used in electrochemical measurements.

The electrochemical measurements were carried out on a three-electrode glass cell with unseparated cathodic and anodic compartments (the working solution volume was from 5 to 15 cm^3) using a universal high-speed potentiostat-galvanostat Autolab/PGSTAT302N (ECOCHEMIE, Netherlands) by CVA and square-wave voltammetry (SWVA). Before experiments, the working solutions were deaerated by alternatively evacuating the electrochemical cells and filling them with argon. During preliminary operations and electrochemical measurements, a small excessive argon pressure (~20 mbar) was maintained over solutions using a vacuum-argon Schlenk line [21, 24–28, 30, 33, 34]. All electrochemical measurements were carried out at room temperature in a neutral aqueous phosphate buffer with pH 7.24; the overall concentration of components was ~0.13 M. The potential scan rate v was in the interval of 0.01–2 V/s; the SWVA measurements were carried out in potential steps of 0.005 V, the amplitude was 0.02 V, and the frequency was 25 Hz. A glassy carbon disk electrode ~0.3 mm in diameter was used as the working electrode. A Pt wire served as the counter electrode. A silver chloride ($Ag/AgCl/KCl_{sat}$) was used as the reference electrode. All potentials are shown with respect to this electrode (except for the specially mentioned cases). Before experiments, the GCE was polished with a diamond suspension (particle diameter ~1 μm, then ~0.25 μm) and then cleaned by sonication. Insofar as DOX adsorbed strongly and irreversibly on the GCE, the electrode was thoroughly cleaned in accordance with recommendations of [9, 35]. This is why, to the standard procedure of electrode preparation, we added the stage of its treatment with the H_2SO_4/H_2O_2 mixture, which was followed by thorough washing with ethanol and triply distilled water. The experimental procedure is described in more detail in [21, 24–28, 30].

The method of dynamic light scattering was used for determination of the hydrodynamic radii R_h of the terpolymer and DOX polymer structures. When preparing the samples to measurements, the aqueous buffers were filtered using a filter with the pore diameter of 0.45 μm. Cuvettes with solution were thermally stabilized at the preset temperature for 20 min. The DLS measurements were carried out using a setup Photocor Compact instrument (Photocor, Russia), equipped with a diode laser with the wavelength of 654 nm. During the analysis of solutions of the terpolymer and DOX polymer structures, the detection angle was 90°. The experimental results were processed using software DynaLS, version 2.8.3. The curves of the size distribution of light scattering centers were obtained by measuring the fluctuations in the intensity of scattering by solutions. The values R_h were determined based on the Einstein–Stokes equation

$$D = kT/6\pi\eta R_h,$$

where D is the diffusion coefficient of a particle, k is the Boltzmann constant, T is the absolute temperature, K, and η is the medium viscosity.

The quantum chemical calculations were carried out by a semi-empirical method AM1 in the software Gaussian 09 [36] based the density functional theory (DFT) (PBE/SBK). Using the program PRIRODA [37], we modeled the copolymer region that contained the number of VP and TEGDMA units in the experimentally found mole ratio maximally suitable for calculations. The optimization of the DOX molecule was also carried out using software Gaussian 09 [36]. The hybrid functional TPSSh and the basis set 6-311++G**//6-31G* were used as the method and the basis. The found geometry was used in modeling the host-guest system. The latter procedure was also carried out by the same methods as those used for the terpolymer regions. In the next stage, during the QTAIM studies of the individual bonds formed and the TDDFT modeling the spectra, we also used the Gaussian 09 software (TPSSh/311++G**//6-31G*).

For the QTAIM analysis of wave functions, we used the program package AIMALL (version 10.05.04) [38]. The wave functions of structures were calculated in the same approximations as the optimization of the geometry of small regions of copolymers. In particular, the analysis of wave functions allowed finding the energy of intermolecular bonds (E_{bd}), the electron density (ρ), and the Laplacian of electron density ($\nabla^2\rho$) in the critical points of the bond. The energy of intermolecular bonds was calculated using the formula $E_{a-b} \approx 1/2v_e(r)$ [39], where E_{a-b} is the A–B bond energy, and $v_e(r)$ is the density of potential energy in the critical point of the A–B bond.

RESULTS AND DISCUSSION

Electrochemistry of Quinones in Protic and Aprotic Media

The main features of the electroreduction (ER) and electrooxidation (EO) of quinones were elucidated to the 1960s, e.g., see [40–42]. For example, the simplest member of the quinone family, *para*-benzoquinone *p*-$O=C_6H_4=O$ is reversibly reduced in nonaqueous solvents in two one-electron stages (Scheme 1) [40–43]:

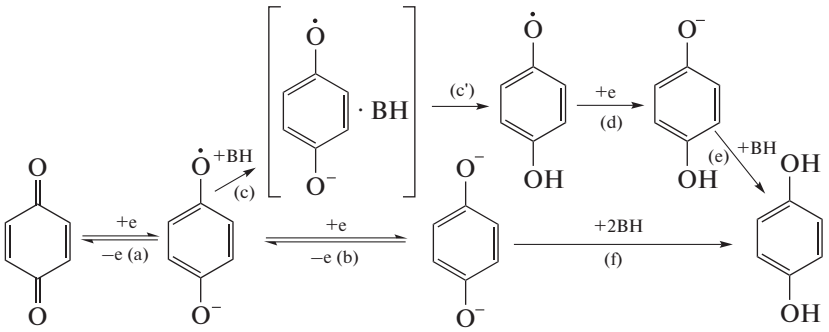

Scheme 1. The overall mechanism of electroreduction of quinones in protic (stages a, c, c', d, e) and aprotic (stages a, b, f) media.

The other quinones are reduced by approximately the same scheme, e.g., naphthoquinone, anthraquinone, and their derivatives. After the transfer of the first electron, the formed radical anion, namely, semiquinone (stage a) adds the second electron to form dianion (stage b). The latter adds protons from the solvent (proton donor BH) to form hydroquinone in the simplest case (stage f). The subsequent transformations of the proton donor are omitted in this scheme. In certain cases, the semiquinone dimerization is not ruled out, this reaction is sufficiently typical of radical anions of aromatic compounds [44].

However, the consecutive individual one-electron reduction steps of quinones are observed only in aprotic media, whereas in protic solvents a single reversible two-electron wave occurs [40, 41, 43]. Insofar as the protonation of negatively charged intermediates and radical species usually precedes the charge transfer [45, 46], the next sufficiently fast process, namely, the formation of a metastable charge-transfer complex intermediate–proton donor (stage c) most probably precedes stage d. The ER potential of quinones in water and water-organic media is pH dependent.

The main relationships of the electroreduction of quinones were found first for the Hg electrode which is used today much more rarely. At the same time, on the mercury electrode it is impossible to study the EO of depolarizers at $E \geq \sim +(0.2–0.4)$ V due to the oxidation of the electrode itself [47]; moreover, during the adsorption of carbonyl compounds on the polarized Hg surface, the formation of organomercury compounds cannot be ruled out [47]. For the electroanalytical determination, especially in combination with liquid chromatography, the solid electrodes are more suitable, because, according to [48], they provide the higher sensitivity and the lower level of background noises.

The electrooxidation was also studied earlier in sufficient detail. The EO of the simplest quinone, viz., hydroquinone, produces nonsoluble quinhydrone in high yield in aqueous media and protonated quinone in aprotic solutions (this stage is not shown in Scheme 2). The mechanism of the ECE process proves to be sufficiently complicated and the obtained results are controversial, especially, the results on the number of involved electrons n, the nature of intermediates and intermediate stages. However, the overall mechanism can be described by Scheme 2 [41–43]:

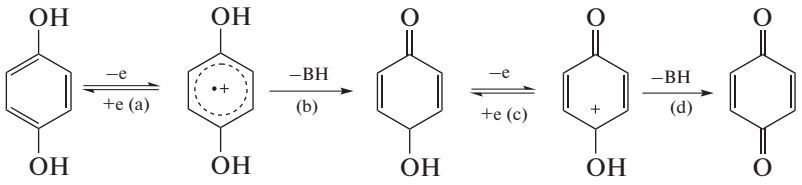

Scheme 2. The overall mechanism of electrooxidation of hydroquinones in aprotic media.

In aprotic media, two reversible one-electron waves are usually assumed which approximately correspond to stages a and c; in protic media, a single two-electron wave either reversible or quasi-reversible is assumed.

Electrode Reactions and Adsorption of DOX in Protic Media on Different Electrodes

The antibiotic of the anthracycline series, doxorubicin (DOX, adriamycin, pK_a 8.6) (8S,10S)-10-(4-amino-5-hydroxy-6-methyl-tetrahydro-2H-piran-2-yloxy)-6,8,11-trihydroxy-8-(2-hydroxyacetyl)-1-methoxy-7,8,9,10-tetrahydrotetracene-5,12-dione pertains to quinone derivatives and is highly active (chemically and electrochemically). The latter is mainly associated with the presence of two reaction centers in its composition, namely, quinone and hydroquinone centers (Fig. 1). DOX is a polar molecule with the high degree of charge delocalization and is a good acceptor of electrons.

Many authors dwelled on the electrochemical properties of DOX [9, 35, 48–65] and its electroanalytical determination [35, 58, 60, 61, 65–74], first of all, on Hg [49–53, 58, 60, 66] and later on several solid electrodes, viz., Au, Ag amalgam, Pt, and various forms of carbon, namely, graphite, pyrolytic graphite (PG), basal plane of pyrolytic graphite (BPPG) [48, 54, 56, 57, 59–61, 65, 67–74], and, above all, the carbon paste electrode (CPE). The faradaic signals on such electrodes are higher as compared with, e.g., the glassy carbon electrode for which substantially less systematic data are known [9, 35, 61, 75]. According to [48–61], in protic media DOX is reduced similarly to classical quinone derivatives, i.e., in a single reversible two-electron wave (Scheme 3; the degree of reversibility of stages is ignored). The reduction involves the quinone groups in positions 5,12 of the anthracycline chromophore [35, 49, 53, 56]. According to [53], the equilibrium potential E^0 of this stage is –0.61 V (pH 7.6), (–0.57 V according to the results of pulse radiolysis [64]; pH 7.0) vs. SCE.

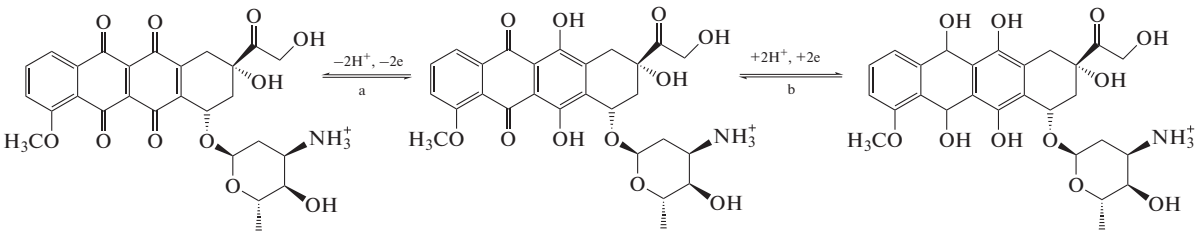

Scheme 3. The overall mechanism of ER and EO of DOX in protic media.

The cathodic voltammetric peak which corresponds to this process bifurcates in neutral media, and a new peak appears at the potential more negative than ~0.03 V if the potential scan rate $v \le 0.01–0.1$ V/s [49, 51, 53]. In acidic media, no bifurcation is observed. The virtually complete reversibility of the electron transfer can be observed only at $v \ge 0.5$ V/s [53]. Similar to other quinones, not only the E_{ER} of DOX is pH dependent but also the character of its ER in water and water-organic media [35, 48, 52, 60, 65]. Thus, on the CPE, the reversible ER was observed only in neutral and strongly acidic regions at pH about 2.3 [48]. The height of this peak in SWVA depended the pH of the medium. Thus, on the Ag amalgam, it was maximum at pH 5–6 in the Britton–Robinson buffer, but several times decreased at pH 7–8 and 2–4 [65]. At pH 4.5, two cathodic peaks were observed one of which was irreversible, whereas in the neutral region, only one peak was observed [48].

The reason for such bifurcation of the cathodic peak is still unknown. Some authors [53] assume that it is caused by deglycosidation (abstraction of the glycoside group from DOX position 7 to form deoxyaglycone), the other authors [49, 50, 52] associate the appearance of two peaks with the reduction two forms of DOX, viz., adsorbed and diffusing from the bulk which have different energy characteristics.

At more negative potentials (–1.18 and –1.41 V) on the mercury electrode, two extra waves were observed, no longer reversible [49]; they were associated with the consecutive one-electron ER of the carbonyl group in position 9 of the side chain.

The electrooxidation involves the dihydroquinone fragment of the molecule in position 6,11 [48]. According to [61], for $v \le 0.01$ V/s, this process is reversible, its potential on the GCE is independent of v in the interval of 0.001–0.01 V/s being equal to about +0.53 V (SCE) (pH 4.5); the close results were obtained in [55] on the BPPG under the same conditions. As v increased, the ER became quasi-reversible and at $v \ge 0.1–0.2$ V/s almost irreversible; thus, the potential difference between anodic and cathodic peaks ΔE at pH 4.5 was about 0.15 V for BPPG [55] and CPE [48]. According to the authors of [55], this means that the rate of electron transfer in the hydroquinone fragment is much lower than in the quinone fragment. This was also confirmed by the results of ac phase-sensitive voltammetry, namely, the effective ER component of the hydroquinone fragment in the redox system turned out to be so small that the authors of [55] failed to obtain any quantitative data even at the frequency of 100 Hz. However, on the CPE (10^{-4} M DOX, Walpole's buffer, pH 4.5, $v = 0.34$ V/s), the ER

Quinone (I) and hydroquinone (II) redox centers

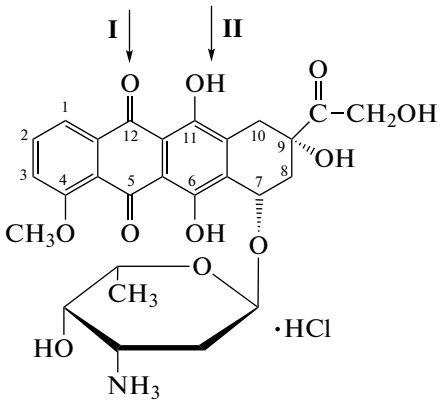

Fig. 1. Doxorubicin structure.

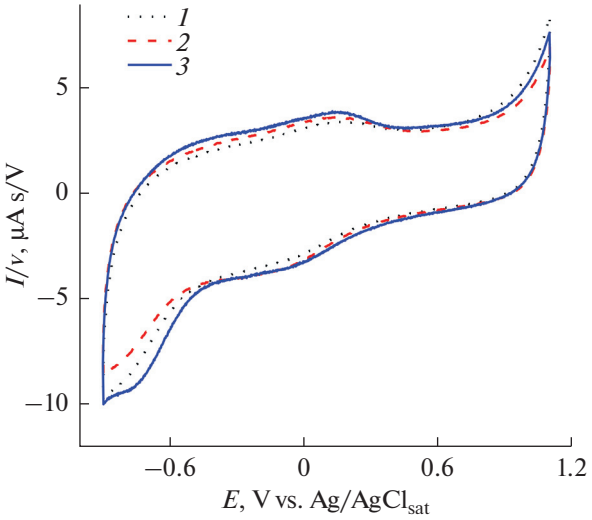

Fig. 2. Comparison of background CVA curves measured at $v = 0.1$ V/s in aqueous phosphate buffer with pH 7.24: (*1*) buffer; (*2*) buffer + 0.3 mg/mL TP; (*3*) buffer + 0.3 mg/mL TP + 8.5×10^{-4} M lactose.

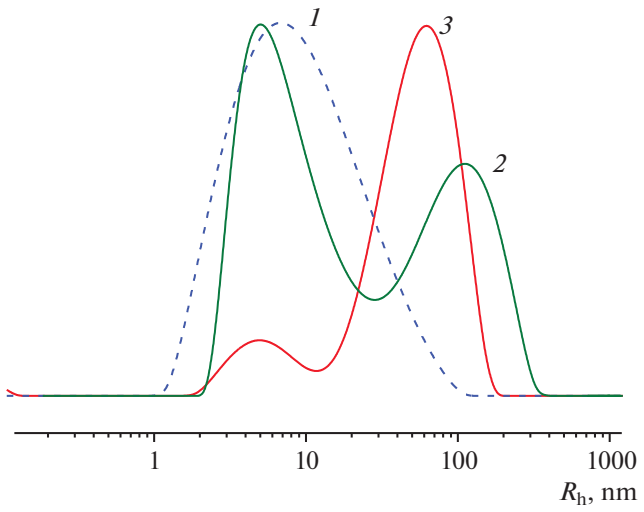

Fig. 3. Light scattering distribution over the particle size in aqueous buffers of (*1*, *2*) terpolymer VP–MAA–DMTEG and (*3*) polymer composite TP–DOX. Concentration of TP: (*1*) 1 and (*2*) 3.5 mg/mL; concentration of TP–DOX composite (*3*) 1 mg/mL, 25°C, pH 7.2–7.4 with additions of NaCl (137 mM) and KCl (2.68 mM).

was irreversible according to [48]. On solid electrodes, the oxidation potential of the hydroquinone fragment of DOX also depended on pH; moreover, dE/dpH ~ 0.06 V [35, 61, 69]. By and large, the CVA curves on different electrodes were much similar, contained cathodic-anodic peaks in the cathodic branch at E about –(0.45–0.65) V and the anodic-cathodic peaks at about +(0.30–0.70) V in the anodic branch, which depended on the pH, the scan rate, the electrolyte nature, and the other experimental conditions [35].

DOX adsorbs well on mercury [50–57] and carbon electrodes, namely, GCE, CPE, etc. [56, 57, 61, 69]. Its limiting coverage on the GC electrode was reached even at the volume concentration of DOX of 9×10^{-7} M [61]. This is why the dependence of the DOX oxidation current on its concentration on a CPE was nonlinear in the interval from 10^{-4} to 10^{-8} M [48]. It was shown that the DOX adsorption on the GCE is irreversible [61]. The authors of [51–55] studied in detail the adsorption behavior of DOX and determined its main parameters on the mercury [51] and PG electrodes [54]. It was shown that on the Hg electrode in the acetate buffer with pH 4.5, the limiting adsorption Γ_∞ in the region of maximum coverage (at $E = -0.2$ V, i.e., near the PZC) $\Gamma_\infty = 1.1 \times 10^{-10}$ mol/cm^2, and the attraction constant a = 1.66 (1.51 at pH 7.6 [54]), which pointed to the presence of strong interactions in the adsorption layer. Note also that DOX itself dissolves better in acidic and alkaline buffers but much more difficultly in neutral solutions and water in which it tends to form associates [76]. However, we have shown that in the concentration interval from 10^{-5} to 10^{-4} M DOX in water, the Buger–Lambert–Ber law is observed, i.e., the compound in solution is in its molecular form or as small aggregates [30].

The Electrochemical Characterization of Background Solutions and the DLS Studies of Buffer Solutions of DOX and TP–DOX

Thus, the electrochemical properties of DOX were studied sufficiently thoroughly, the literature data formed the basis of our study and allowed us to select the optimal conditions for measurements. For instance, we carried out all experiments in the aqueous phosphate buffer taking into account its closeness to the physiological pH (7.2–7.4). The binding constants of DOX with various carriers (e.g., with dextrin derivatives [9]) at these pH values are higher than at pH < 7.

Insofar as in this study we used not individual doxorubicin hydrochloride but its commercial drug, before carrying out our studies, it was necessary to check separately the electrochemical and adsorption properties of this drug and each additive, especially the filler, i.e., lactose monohydrate, as well as their effect on the voltammetric characteristics of DOX. The CVA curves of the background solutions of different composition were obtained under the same conditions as for the DOX itself in its encapsulated and free forms, i.e., in the potential interval from –1.0 to +1.1 V at the potential scan rate of 0.02–2 V/s (Fig. 2). It is evident that all the curves lack any specific features[2]. Moreover, the CVA curves almost coincided in pure buffer, in the presence of TP, and with addition of lactose.

The TP and TP-DOX solutions were studied by the DLS method. Figure 3 shows the distribution curves

[2] Sometimes, near –0.7 V, a small cathodic peak appeared ($i_{max} \leq$ 0.02 μA) probably associated with oxygen traces which were difficult to remove. After the solution was thoroughly blown through, the peak disappeared; oxygen was removed more easily from solutions containing encapsulated DOX.

Table 1. Potentials of cathodic (E_{pc1}, E_{pc2}) and anodic (E_{pa1}, E_{pa2}) peaks (V) of DOX and TP-DOX structures, the potential difference ΔE, the formal redox potentials $E^0_{pc1/pa1}$ and $E_{pa2/pc2}$ determined in different potential intervals and for different scan directions, $v = 0.1$ V/s

Depolarizer	E_p, V (from Fig. 5). E interval from −0.8 to +0.8 V, scan direction −0.1 → +0.8 → −0.8 V							
	E_{pc1}	E_{pa1}	ΔE	$E^0_{pc1/pa1}$	E_{pa2}	E_{pc2}	ΔE	$E_{pa2/pc2}$
DOX	−0.601	−0.571	0.030	−0.586	0.586	0.245	0.341	0.416
DOX + TP	−0.586	−0.554	0.032	−0.570	0.556	0.312	0.244	0.434
	E_p, V (from Figs. 6a, 6b). Cathodic scan interval from −0.2 to −0.8 V*				E_p, V (from Figs. 9a, 9b). Anodic scan interval from −0.2 to +0.8 V**			
DOX	−0.611	−0.583	0.028	−0.597	0.556	0.245	0.311	0.401
DOX + TP	−0.599	−0.544	0.055	−0.572	0.614	0.198	0.416	0.406

* Scan direction: −0.1 → −0.8 → 0 V.

** Scan direction −0.1 → +0.8 → −0.2 V.

of the intensity of light scattering over the size of TP particles at the low and medium concentrations of the terpolymer in phosphate buffers with pH 7.2–7.4. In the size interval of 0.1–1000 nm, in a dilute solution of terpolymer, only one peak was present; in its maximum, R_h was about 7 nm. In the more concentrated solution, the second peak with R_h ~100 nm appeared and the distribution became bimodal. These peaks should be attributed to individual molecules and their aggregates, respectively. The distribution curves in a solution of the DOX polymer composite was substantially different: the second peak shifted to the lower R_h (~66 nm) and its intensity increased, which suggested that the DOX polymer structure was present in solution and was stable in the temperature interval studied (25–45°C). The DLS data pointed to the formation of the guest–host structure as a result of penetration of DOX molecules into the cavities in terpolymer nanoparticles. It is known [77] that in such nanosystems, a large number of very different and practically useful electrode processes occur and their mechanism may differ from that in individual solutions.

The Comparative Electrochemical Study of DOX forms: Free and TP-Encapsulated

After the detailed characterization of the background and the determination of the E region of ideal polarizability, we carried out a comparative study of free and terpolymer-encapsulated DOX by the CVA and SWVA methods. Here, we show mainly the results obtained in the first potential scans. It is evident that the electrode process proceeded by the general mechanism typical of the reduction–oxidation of quinone compounds to which DOX pertains. In the potential interval from −1 to +1, the CVA curves contained two pairs of two-electron redox peaks which more probably corresponded to the irreversible (or, probably, quasi-reversible) anodic oxidation (pa2/pc2) in the interval +(0.3–0.6) V and the almost reversible cathodic reduction of DOX (pc1/pa1) at E near −0.6 V (Fig. 4a), which by and large agreed with the literature data for the majority of electrodes [35, 48–61, 69]. In the cathodic scan at the scan rate ≤0.5 V/s, two weakly pronounced ER peaks were observed which at $v \geq 0.5$–1 V/s merged together to give a single peak also well resolved. The reverse anodic CVA branch always contained only one well pronounced peak. Insofar as the scan rate and, correspondingly, the height of peaks changed sufficiently widely and in the summary figure the curves merged together at the medium and, especially, small v, for the sake of clarity and to reveal the nature of electrode processes (diffusion, adsorption, diffusion-adsorption), these I vs. E dependences (Figs. 4a, 4b) were additionally plotted in different coordinates: I/v vs. E (Figs. 4c, 4d) and $I/v^{0.5}$ vs. E (not shown).

The electrochemical behavior of DOX and the TP-DOX nanostructure somewhat differed from one another (Figs. 4a, 4b). To make their comparison easier, in Fig. 5, we show the curves from Figs. 4a and 4b measured at $v = 0.1$ V/s. It is evident that peak pc1 shifts to the more negative potential and peak pa1 shifts to the less negative potential, i.e., the ER of DOX in the composite (pc1) proceeds more difficultly as compared with the free form, whereas the reoxidation (pa1) proceeds somewhat easier although their ΔE are sufficiently close, see Table 1. Thus, both for free and encapsulated forms, the pair of peaks pc1/pa1 corresponds to the reversible ER/EO of the adsorbed species [78, 79]. In the anodic region, the situation is the opposite, namely, peak pc2 shifts to more positive potentials and peak pa2 shift to less positive potentials (Fig. 4, Table 1). Hence, in the polymer structure, the reduction (pc1)/reoxidation (pa1) of the quinone fragment of DOX is hindered. The oxidation of the hydroquinone center (pa2) and its reverse reduction (pc2) proceed considerably easier. This may be due to

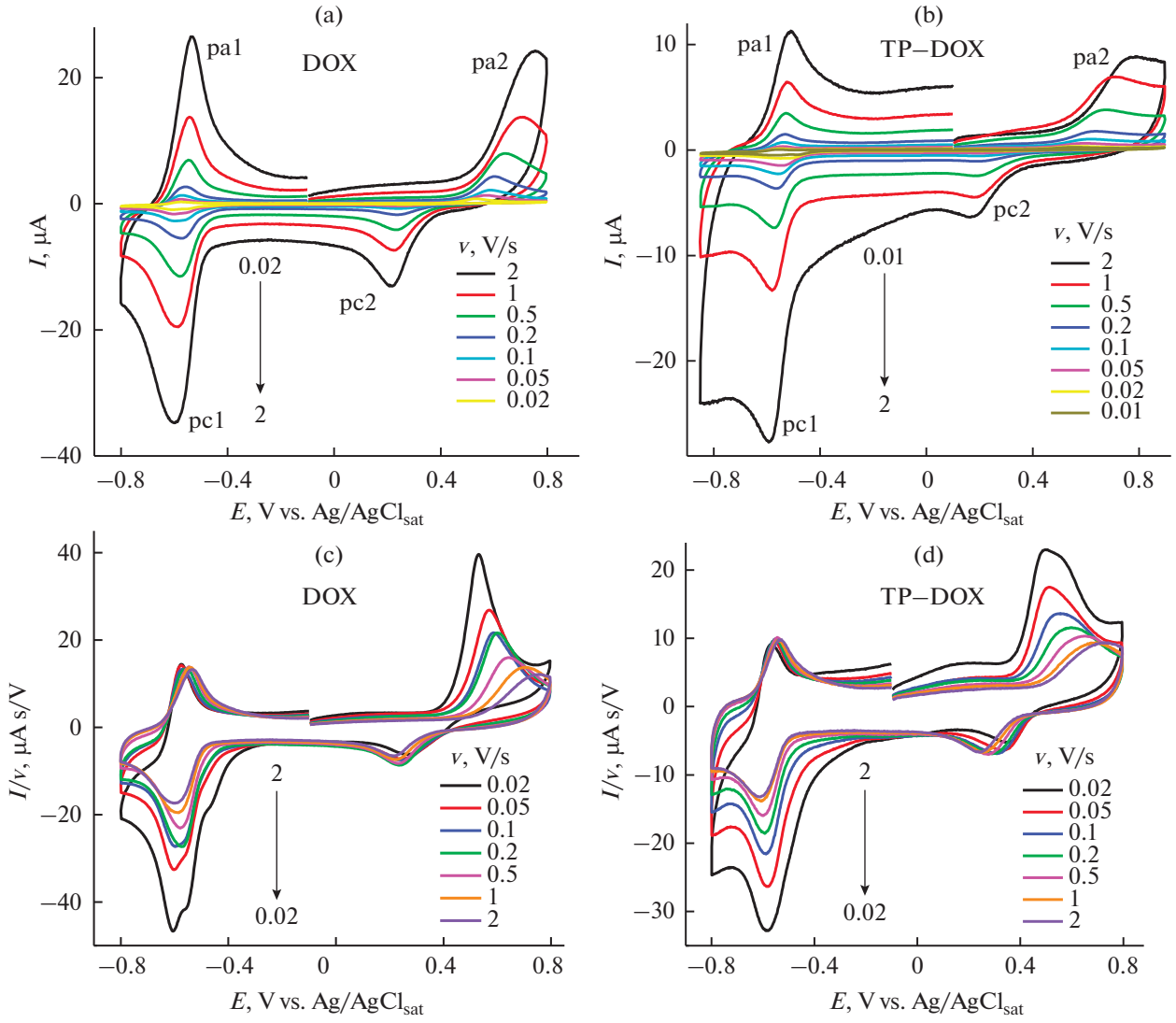

Fig. 4. CVA curves of (a) DOX and (b) TP–DOX in aqueous phosphate buffer (pH 7.24) on a GC electrode in *I* vs. *E* coordinates at potential scan rate $v = 0.01–2$ V/s. DOX concentration (a) 4.0×10^{-5} and (b) 1.4×10^{-5} M; (c) and (d) are the curves (a) and (b) plotted in coordinates *I*/*v* vs. *E*. The 1st scan.

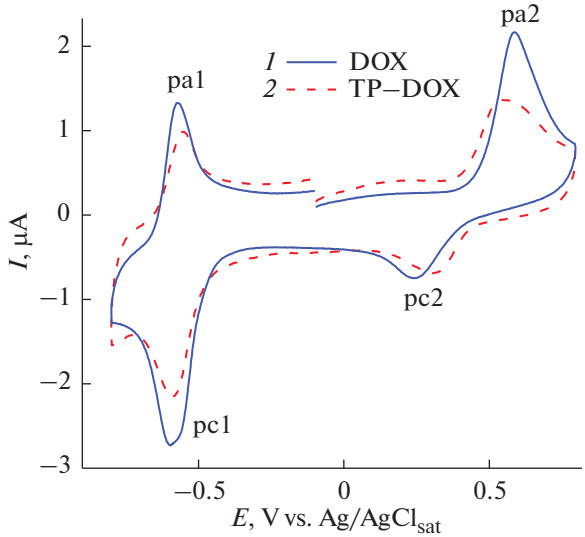

Fig. 5. CVA curves of (*1*) DOX and (*2*) TP–DOX taken from Figs. 4a and 4b. $v = 0.1$ V/s.

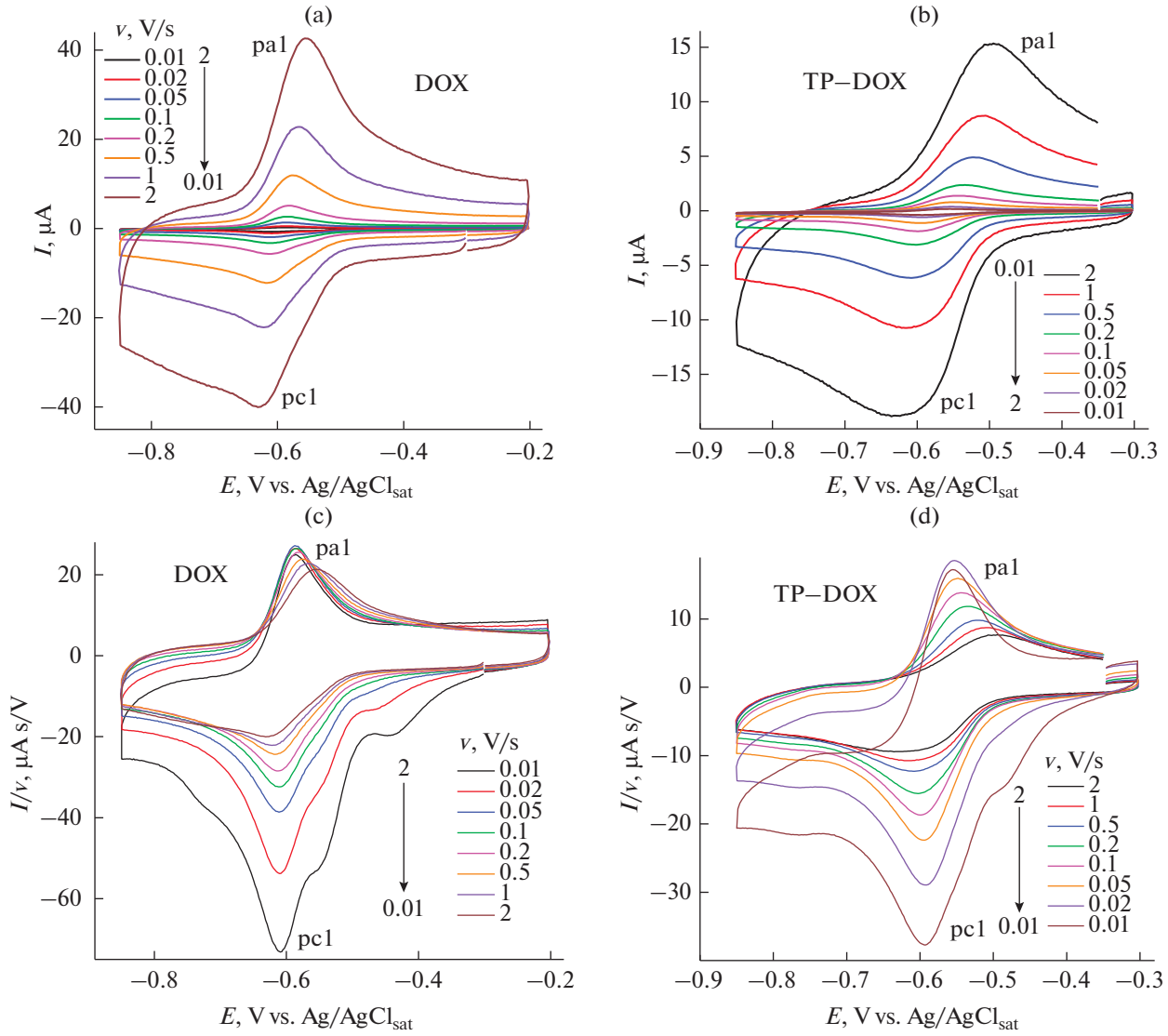

Fig. 6. CVA curves of (a) DOX and (b) TP–DOX structure in the region of cathodic potentials in aqueous phosphate buffer (pH 7.24) on the GC electrode in coordinates I vs. E at scan rates v 0.01–2 V/s. DOX concentration (a) 3.9×10^{-5} and (b) 3.5×10^{-5} M; (c) and (d) curves (a) and (b) plotted in coordinates I/v vs. E. The 1st scan.

the involvement of these groups in the formation of the hydrogen bond, its stretching and weakening. In other words, the oxidation of the encapsulated form proceeds more easily and its reduction proceeds more difficultly, although the potential difference does not exceed several tens mV.

The comparison of Figs. 4a, 4c, and 4b, 4d shows that the bifurcation is less pronounced for the cathodic peak pc1 of encapsulated DOX at low scan rates. Taking the point of view of the authors of [53] that this bifurcation is caused by the fast deglycolization after the transfer of two electrons and the parallel reduction of this product at close E, it should be assumed that the process is complicated in the DOX polymeric nanostructure. In CVA measured in the narrower E interval from –0.2 to –0.9 V, i.e., in the region of the cathodic pair of peaks (Figs. 6a–6d), the bifurcation of the cathodic peak pc1 was practically unobserved. The bifurcation was also weakly pronounced for the lowest volume concentrations of DOX (below 10^{-5} M).

In this regard, the SWVA data turned out to be even more illustrative. Figure 7 shows the corresponding curves for DOX and the TP–DOX structure in the same potential interval as in Fig. 6, which were measured at different frequencies (F = 1–25 Hz) (a, c) and then, for the sake of clarity, normalized to the equal height (b, d). The changes in the shape and position of the cathodic peak near –0.6 V are evident: at the maximum frequency (25 Hz) the peak at –0.58 V prevails and at the minimum frequency (1 Hz) the peak at

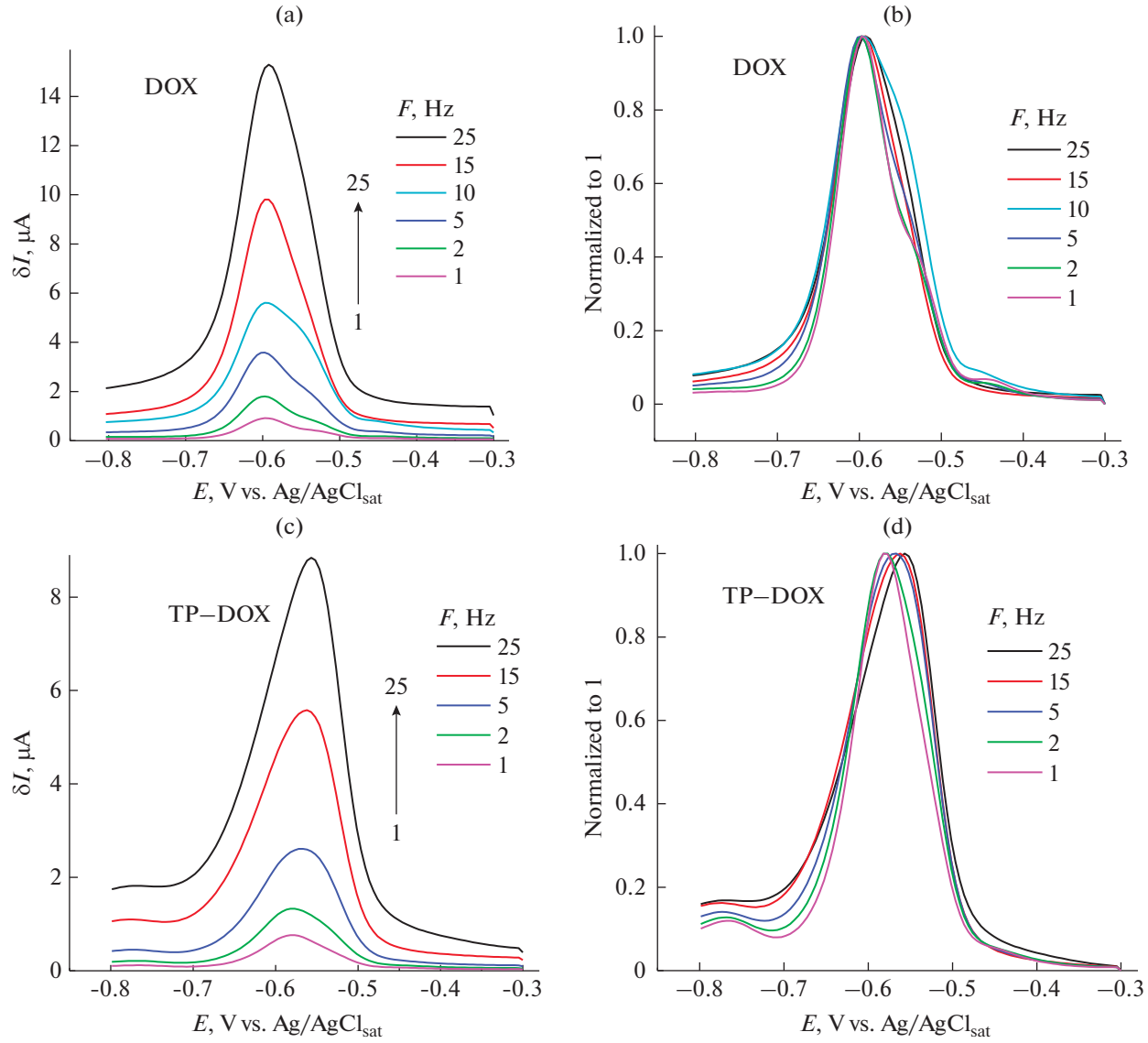

Fig. 7. SWVA of (a) DOX and (c) TP–DOX structure measured at different frequencies and (b, d) normalized to 1. DOX concentration (a) 3.9×10^{-5} and (c) 3.5×10^{-5} M.

–0.56 V is higher. For the free DOX form, this is less pronounced; however, the deviations at low frequencies (1–10 Hz) are visible.

Changes in the Energy Characteristics upon the Transition from the Free DOX Form to Its TP-Encapsulated Form

As we pass from free DOX to its encapsulated form, the nature of the electrode process also changes. It transforms from the purely adsorption process for free DOX to the mixed adsorption–diffusion process for DOX within the TP composite. This follows from the slopes of dependences in Figs. 6a and 6b plotted in coordinates $\log I_{pc1}$ vs. $\log v$ (0.82–0.87 and 0.74–0.76, respectively, Fig. 8).

When analyzing the CVA curves in Figs. 4 and 6, it should be noted, first of all, that they all are not of the purely diffusion nature, otherwise all I vs. E dependences should have coincided in the coordinates $I/v^{0.5}$ vs. E (is not shown). However, in place of their coincidence, we observed only their closeness for DOX at the lowest scan rates, namely, at 0.02 and 0.05 V/s, and only for the pc1 in the cathodic scan, whereas for the anodic reoxidation peak pa1 the coincidence was totally absent. For encapsulated DOX, we observed even no closeness of CVA. As to the analogous dependences in the I/v vs. E coordinates, they were of the purely adsorption nature and coincided only at the maximum scan rates, namely, at 1 and 2 V/s (Figs. 4c, 4d and 6c, 6d). The dependences of the height of cathodic peak I_{pc1} on the scan rate ($\log I_{pc1}$ vs. $\log v$)

obtained in the series of measurements for both systems had the slope close to 1, i.e., about 0.80–0.94, which was typical of the mixed adsorption-diffusion control for the depolarizer transport to the electrode (a part of data is shown in Fig. 8). Or, more exactly, this was typical of an electrode process controlled by adsorption with an insignificant contribution of diffusion. As to the anodic peak of reoxidation pa1 and the cathodic peak of rereduction pc2, their heights in coordinates I vs. v were approximately equal at all scan rates v. This also meant that the process was reversible and its intermediates formed at the potentials corresponding to peaks pc1 and pa2 reacted from the adsorbed state; moreover, this conclusion was valid for both free and encapsulated DOX. It was already noted above that many authors pointed to the fact that the ER of DOX occurred preferentially from the adsorbed state.

Figure 9 shows the CVA curves for the pair of anodic-cathodic peaks pa2 and pc2, which were obtained in a narrow interval of anodic potentials, namely, from +0.1 to +0.9 V (TP–DOX) and from –0.4 to +0.9 V (DOX) in the anodic scan. We observed the same relationships as for the CVA curves in the wide potential interval, namely, by their character, the cathodic peak pc2 and the anodic peak pa2 were close to adsorption peaks at the low scan rates ($v \geq 1$–2 V/s), whereas peak pa2 was close to a diffusion peak at the lowest scan rates ($v \leq 0.05$–0.02 V/s); in the intermediate v region, a mixed adsorption-diffusion process was observed (Fig. 9b). The cathodic peak pc2 did not look as a diffusion peak for all v, the effect of adsorption was stronger for this peak (Fig. 9b).

The Potentials of Redox Pairs pc_1/pa_1 and pc_2/pa_2; the Energy of H Bonds between O Atoms in TP and H atoms in DOX

The results in Figs. 4, 6, 9 were used below for assessing the formal redox potentials E^0 of cathodic (pc_1/pa_1) redox reactions of DOX and TP–DOX (Table 1) under the assumption that $n = 2$ and also of quantities $E_{pa2/pc2}$ at $v = 0.1$ V/s. As seen from Table 1, the cathodic pair of peaks pc_1/pa_1 corresponds indeed to a reversible redox process that proceeds from the adsorbed state (ΔE ~0.03 V). The ratio of peaks I_{pc1}/I_{pa1} is also close to 1 (Fig. 8b), in contrast to the anodic pair of peaks pc2/pa2, and $\Delta E >$ (0.2–0.4) V.

It is also evident that the quantities $E^0_{pc1/pa1}$ and $E_{pc2}/_{pa2}$ for the systems DOX and TP-DOX somewhat differ. In this case, the initial potential is important as well as the scan interval. We assume that this is associated with the formation of complexes TP–DOX. To elucidate the possible nature of these complexes, we carried out the quantum chemical modeling of their structure. As was shown by the quantum-chemical calculations, the hydrogen bonds of various strength

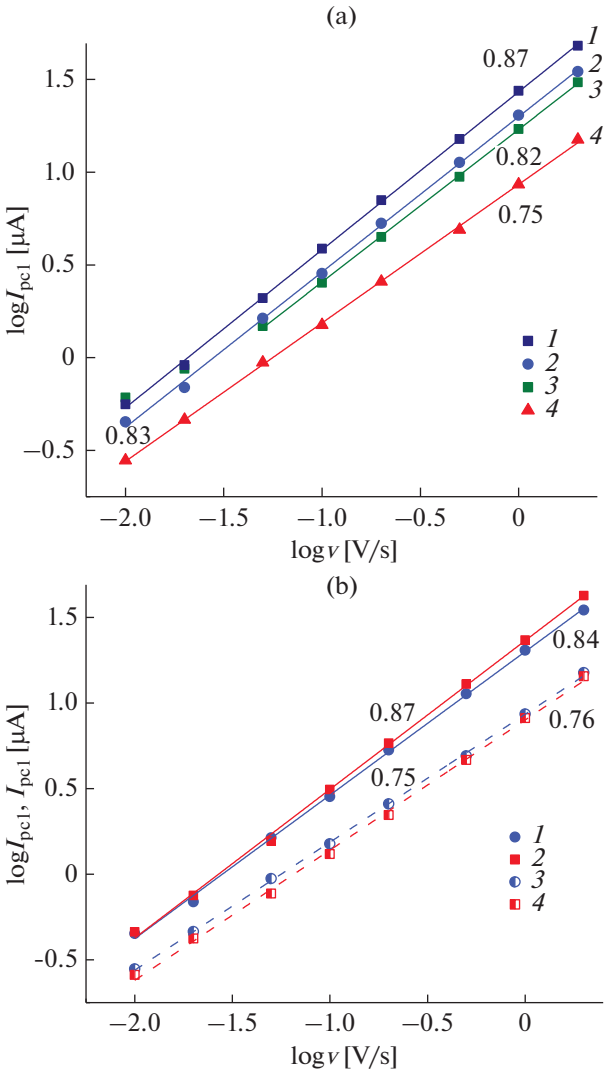

Fig. 8. (a) Dependence of cathodic peaks I_{pc1} on the scan rate ($\log I_{pc1}$ vs. $\log v$) for DOX of different concentration: (*1*) 1.43×10^{-5}, (*2*) 3.5×10^{-6}, (*3*) 3.9×10^{-5} M and (*4*) TP–DOX 3.5×10^{-5} M. (b) Dependences of the height of (*1*, *3*) cathodic I_{pc1} (*2*, *4*) anodic I_{pa1} peaks on the scan rate ($\log I_{pc1}$, I_{pa1} vs. $\log v$) for (*1*, *2*) 3.5×10^{-6} M DOX and (*3*, *4*) 3.5×10^{-5} M TP–DOX. Numbers at the curves indicate their slopes. The capacitive current is subtracted.

and energy can be formed between the electron-donating oxygen-containing groups in the terpolymer and hydrogen in OH and NH_3^+ groups of DOX. In the TP–DOX complex, the units of methacrylic acid are the main donor of electron density and form the strongest bonds with DOX: the energy of the H-bond E_{bd} is in the interval 9–26 kcal/mol, which is comparable with E_{bd} of the carbonyl group of the lactam cycle in VP (7–12 kcal/mol) [80], Table 2. It was shown that the units of the TEGDM copolymer also take part in the formation of TP–DOX complexes; however, the

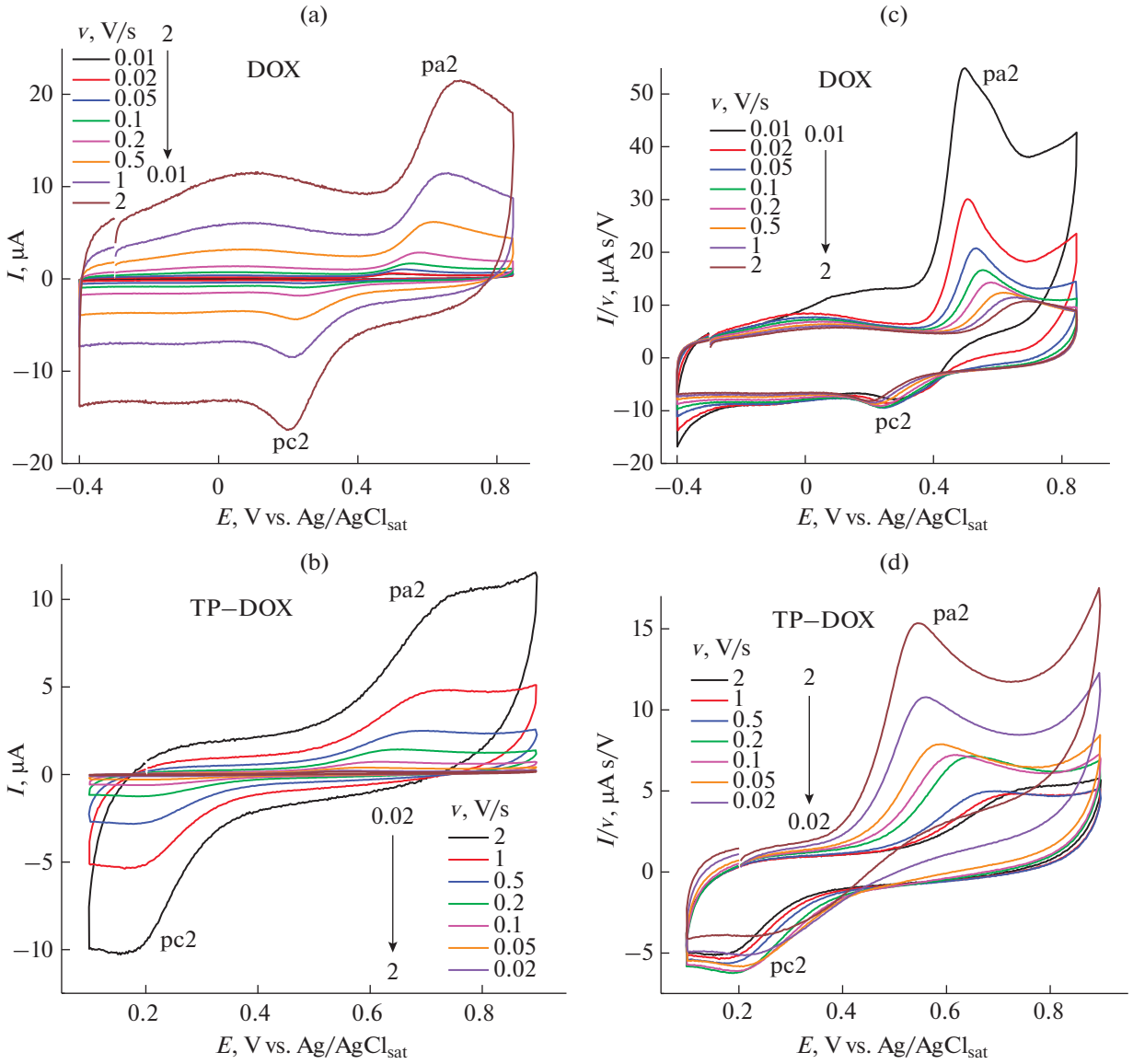

Fig. 9. CVA curves of (a, b) DOX and (c, d) TP–DOX in the region of anodic potentials in aqueous phosphate buffer (pH 7.24) on the GC electrode in coordinates I vs. E at scan rates v 0.01–2 V/s. DOX concentration (a) 3.9×10^{-5} and (b) 3.5×10^{-5} M; (c) and (d) are the curves (a) and (b) plotted in coordinates I/v vs. E. The 1st scan.

energy of hydrogen bonds is lower in this case. According to calculations, the hydrogen bonds between O atoms of DOX and H atoms of copolymer are even weaker and do not exceed 3 kcal/mol. In other cases, the bond energies in such nanostructures can be much higher. Thus, the DFT calculations [81] showed that in the composite DOX–SiO_2–*N*-(phosphomethyl)iminoacetic acid they can exceed 70 kcal/mol, e.g., when the hydrogen bond is formed between hydroxyl of the phosphonium group and hydroxyl at the C(9) atom of DOX (ignoring the additional coordination over silanol groups).

Thus, as follows from the CVA data, the small differences in energy characteristics of the free and encapsulated forms of DOX are not surprising. Nonetheless, it can be assumed that the formation of such a complex should lower the total cytotoxicity and nonselectivity of DOX and, upon its penetration into the cancer cell, may slow down the DOX liberation from the complex.

The difference in the energy characteristic of the bound and free DOX forms was also observed, e.g., in [71] when studying the interaction of DOX with the DNA of calf's thymus using differential pulse voltammetry. It was shown [71] that in the absence of DNA, DOX (10^{-5} M) was oxidized on GCE at +0.41 V (SCE) (pH 7.4, neutral phosphate buffer +0.05 M NaCl, $v = 0.033$ V/s) and reduced at about –0.5 V. The

Table 2. Energy of hydrogen bonds formed between O atoms of TP and H atoms of DOX

TP unit	Electron-donating groups of TP	Electron-withdrawing groups in DOX	E_{bd} (QTAIM), kcal mol^{-1}
MAA	Carboxyl	CH, OCH_3, OH^-, NH_3^+	8.8; 13.3; 12.3; 25.5; 22.1
VP	Carbonyl group of the lactam cycle of VP	OH, OCH_3, NH_3^+	11.8; 9.4; 6.9
DMTEG	Ester group	OH^-	1.2; 1.3; 3.5; 6.2

additions of DNA led to the formation of the DNA–DOX adduct, which shifted the ER potentials in the positive direction as compared with free DOX ($\Delta E_{ER} = 0.04$ V). The ability of DOX to bind DNA not too strongly was demonstrated also using electrochemiluminescence [82]. The electrochemical control tuned out even more efficient in revealing the covalent addition of DOX to magnetic nanoparticles (mixed nickel–zinc ferrites $Ni_{0.5}Zn_{0.5}Fe_2O_4$) which were also used as the carriers of medicinal drugs. Using the CVA method, it was shown that the form of peaks and their potential considerably differed for free and covalently bound DOX forms; the piezoelectric weighing made it possible to quantitatively assess DOX covalently bound with the surface of nanoparticles [75].

CONCLUSIONS

Thus, the energy characteristics differ for free doxorubicin and doxorubicin encapsulated into the terpolymer *N*-vinylpyrrolodone-methacrylic acid-triethylenglycol dimethacrylate in aqueous buffers. Based on results of cyclic voltammetry and quantum-chemical modeling, it is concluded that DOX binds with the terpolymer by numerous H bonds of different length and energy. Apparently, this give rise to changes in the corresponding redox potentials E^0. Moreover, the character of the electrode process changes from the almost adsorption process for free DOX to the adsorption–diffusion process for DOX within its polymeric complex. From these results, it follows that the incorporation of DOX into a polymer structure may lower the total toxicity of this rather nonselective drug and provide its targeted delivery into diseased cells followed by its subsequent prolonged release/controlled liberation. It can be assumed that such an approach may be also useful for other medicinal drugs.

FUNDING

The study was supported by the State Grants 124020500019-2, 124013000692-4.

CONFLICT OF INTEREST

The authors of this work declare that they have no conflict of interest.

REFERENCES

1. Tacar, O., Sriamornsak, P., Crispin, R., and Dass, C.R., Doxorubicin: an update on anticancer molecular action, toxicity and novel drug delivery systems, *J. Pharm. Pharmacol.*, 2013, vol. 65, p. 157. https://doi.org/10.1111/j.2042-7158.2012.01567.x
2. Minotti, G., Menna, P., Salvatorelli, E., Cairo, G., and Gianni, L., Anthracyclines: Molecular advances and pharmacologic developments in antitumor activity and cardiotoxicity, *Pharm. Rev.*, 2004, vol. 56, p. 185. https://doi.org/10.1124/pr.56.2.6
3. Tmejova, K., Hynek, D., Kopel, P., Dostalova, S., Smerkova, K., Stanisavljevic, M., Hoai, V.N., Nejdl, L., Vaculovicova, M., and Krizkova, S., Electrochemical behaviour of doxorubicin encapsulated in apoferritin, *Int. J. Electrochem. Sci.*, 2013, vol. 8, p. 12658.
4. Mishra, A.K., Lim, J., Lee, J., Park, S., Seo, Y., Hwang, H., and Kim, J.K., Control drug release behavior by highly stable and pH sensitive poly(*N*-vinylpyrrolidone)-*block*-poly(4-vinylpyridine) copolymer micelles, *Polymer*, 2021, vol. 213, p. 123329. https://doi.org/10.1016/j.polymer.2020.123329
5. Sudareva, N., Suvorova, O., Saprykina, N., Vlasova, H., and Vilesov, A., Doxorubicin delivery systems based on doped CaCO3 cores and polyanion drug conjugates, *J. Microencapsulation*, 2021, vol. 38, p. 164. https://doi.org/10.1080/02652048.2021.1872724
6. Torchilin, V.P., Recent approaches to intracellular delivery of drugs and DNA and organelle targeting, *Ann. Rev. Biomed. Eng.*, 2006, vol. 8, p. 343. https://doi.org/10.1146/annurev.bioeng.8.061505.095735
7. Rumyantseva, S.S. and Bukreeva, T.V., Controlling the permeability of polyelectrolyte capsule shells by modifying them with haematin, *Colloid J.*, 2019, vol. 81, p. 446. https://doi.org/10.1134/S1061933X19040148
8. Trushina, D.B., Akasov, R.A., Khovankina, A.V., Borodina, T.N., Bukreeva, T.V., and Markvicheva, E.A., Doxorubicin-loaded biodegradable capsules: Temperature induced shrinking and study of cytotoxicity in vitro, *J. Mol. Liq.*, 2019, vol. 284, p. 215. https://doi.org/10.1016/j.molliq.2019.03.152
9. Swiech, O., Majdecki, M., Garbacz, P., Gwardys, P., and Bilewicz, R., Impact of pH and cell medium on the interaction of doxorubicin with lipoic acid cyclodextrin conjugate as the drug carrier, *J. Incl. Phenom. Macrocycl. Chem.*, 2020, vol. 97, p. 129. https://doi.org/10.1007/s10847-020-00994-z
10. Manchun, S., Dass, C.R., and Sriamornsak, P., Stability of freeze-dried pH-responsive dextrin nanogels con-

taining doxorubicin, *Asian J. Pharm. Sci.*, 2016, vol. 11, p. 648. https://doi.org/10.1016/j.ajps.2015.09.006

11. Ma, B., Zhuang, W., Wang, Y., Luo, R., and Wang, Y., pH-sensitive doxorubicin-conjugated prodrug micelles with charge-conversion for cancer therapy, *Acta Biomater.*, 2018, vol. 70, p. 186. https://doi.org/10.1016/j.actbio.2018.02.008
12. Gonçalves, M., Mignani, S., Rodrigues, J., and Tomás, H., A glance over doxorubicin based-nanotherapeutics: From proof-of-concept studies to solutions in the market, *J. Controlled Release,* 2020, vol. 317, p. 347. https://doi.org/10.1016/j.jconrel.2019.11.016
13. Gutierrez-Pineda, E., Rocio Caceres-Velez, P., Jose Rodriguez-Presa, M., Moya, S.E., Gervasi, C.A., and Amalvy, J.I., Hybrid conducting composite films based on polypyrrole and poly(2-(diethylamino)ethyl methacrylate) hydrogel nanoparticles for electrochemically controlled drug delivery, *Adv. Mater. Interfaces,* 2018, vol. 5, p. 1800968. https://doi.org/10.1002/admi.201800968
14. Chen, K., Cai, H., Zhang, H., Zhu, H., Gu, Z., Gong, Q., and Luo, K., Stimuli-responsive polymer-doxorubicin conjugate: Antitumor mechanism and potential as nano-prodrug, *Acta Biomater.*, 2019, vol. 84, p. 339. https://doi.org/10.1016/j.actbio.2018.11.050
15. Santos, R., Cardoso, S., Correia, S., Oliveira, P.J., Santos, M.S., and Moreira, P.I., Doxorubicin: The good, the bad and the ugly effect, *Curr. Med. Chem.*, 2009, vol. 16, p. 3267. https://doi.org/10.2174/092986709788803312
16. Folttmann, H. and Quadir, A., Polyvinylpyrrolidone (PVP)—One of the most widely used excipients in pharmaceuticals: An overview, *Drug Deliv. Technol.*, 2008, vol. 8, p. 22.
17. Wang, J., Wang, G., Sun, Y., Wang, Y., Yang, Y., Yuan, Y., Li, Y., and Liu, C., In Situ formation of pH-/thermosensitive nanohybrids via friendly-assembly of poly(*N*-vinylpyrrolidone) onto LAPONITE®, *RSC Adv.*, 2016, vol. 6, p. 31816. https://doi.org/10.1039/C5RA25628C
18. Ramalingam, V., Varunkumar, K., Ravikumar, V., and Rajaram, R., Target delivery of doxorubicin tethered with PVP stabilized gold nanoparticles for effective treatment of lung cancer, *Sci. Rep.*, 2018, vol. 8, p. 1. https://doi.org/10.1038/s41598-018-22172-5
19. Kurmaz, S.V., Obraztsova, N.A., Balakina, A.A., and Terent'ev, A.A., Preparation of the amphiphilic copolymer of *N*-vinylpyrrolidone with triethylene glycol dimethacrylate nanoparticles and the study of their properties *in vitro, Russ. Chem. Bull.*, 2016, vol. 65, p. 2097. https://doi.org/10.1007/s11172-016-1558-x
20. Kurmaz, S.V., Fadeeva, N.V., Soldatova, Y.V., Faingold, I.I., Poletaeva, D.A., Ignat'ev, V.M., Emel'yanova, N.S., Shilov, G.V., and Kotelnikova, R.A., New complexes of metformin based on the copolymer of *N*-vinylpyrrolidone with triethylene glycol dimethacrylate and their activity in experimental type 2 diabetes mellitus, *J. Polym. Res.,* 2021, vol. 28, p. 345. https://doi.org/10.1007/s10965-021-02684-x
21. Kurmaz, S.V., Sen', V.D., Kulikov, A.V., Konev, D.V., Kurmaz, V.A., Balakina, A.A., and Terent'ev, A.A., Polymer nanoparticles of *N*-vinylpyrrolidone loaded with an organic aminonitroxyl platinum(IV) complex. Characterization and investigation of their in vitro cytotoxicity, *Russ. Chem. Bull.,* 2019, vol. 68, p. 1769. https://doi.org/1066-5285/19/6809-1769
22. Kurmaz, S.V., Fadeeva, N.V., Fedorov, B.S., Kozub, G.I., Emel'yanova, N.S., Kurmaz, V.A., Manzhos, R.A., Balakina, A.A., and Terentyev, A.A., New antitumor hybrid materials based on Pt^{IV} organic complex and polymer nanoparticles consisting of *N*-vinylpyrrolidone and (di)methacrylates, *Mendeleev Commun.*, 2020, vol. 30, p. 22. https://doi.org/10.1016/j.mencom.2020.01.007
23. Kurmaz, S.V., Fadeeva, N.V., Fedorov, B.S., Kozub, G.I., Kurmaz, V.A., Ignat'ev, V.M., and Emel'yanova, N.S., Amphiphilic copolymers of *N*-vinylpyrrolidone with (di)methacrylates as promising carriers for the platinum(IV) complex with antitumor activity, *Russ. Chem. Bull.*, 2021, vol. 70, p. 1832. https://doi.org/10.1007/s11172-021-3289-x
24. Kurmaz, S.V., Konev, D.V., Kurmaz, V.A., Kozub, G.I., Ignat'ev, V.M., Emel'yanova, N. S., Balakina, A.A., and Terentyev, A.A., New nanosize systems with antitumor activity based on the Pt(IV) complexes with nicotinamide ligands and amphiphilic copolymers of *N*-vinylpyrrolidone and (di)methacrylate, *INEOS Open*, 2021, vol. 4, p. 195. https://doi.org/10.32931/io2123a
25. Kurmaz, S.V., Konev, D.V., Sen', V.D., Kurmaz, V.A., and Kulikov, A.V., Preparation and characterization of stable water soluble hybrid nanostructures of hydrophobic compounds by encapsulation into nanoparticles of amphiphilic *N*-vinylpyrrolidone copolymers of new generation, *IOP Conf. Ser.: Mater. Sci. Eng.*, 2020, vol. 848, p. 012043. https://doi.org/10.1088/1757-899X/848/1/012043
26. Kurmaz, S.V., Gak, V.Yu., Kurmaz, V.A., and Konev, D.V., Preparation and properties of hybrid nanostructures of zinc tetraphenylporphyrinate and an amphiphilic copolymer of *N*-vinylpyrrolidone in a neutral aqueous buffer solution, *Russ. J. Phys. Chem. A,* 2018, vol. 92, p. 329. https://doi.org/10.1134/S0036024418020152
27. Kurmaz, S.V., Fadeeva, N.V., Gorshkova, A.I., Kurochkin, S.A., Knerelman, E.I., Davydova, G.I., Torbov, V.I., Dremova, N.N., Kurmaz, V.A., Konev, D.V., Ignatiev, V.M., and Emelyanova, N.S., Mesoporous networks of *N*-vinylpyrrolidone with (di)methacrylates as precursors of ecological molecular-imprinted polymers, *Materials*, 2021, vol. 14, p. 6757. https://doi.org/10.3390/ma14226757
28. Kurmaz, S.V., Kurochkin, S.A., Knerelman, E.I., Davydova, G.I., Torbov, V.I., Dremova, Konev, D.V., Kurmaz, V.A., and Emelyanova, N.S., Mesoporous networks of *N*-vinylpyrrolidone with (di)methacrylates as efficient precursors of ecological molecular imprinted polymers, in: *Prime Archives in Material Science*: 4th Edition, Esubalew Kasaw Gebeyehu, Ed., Hyderabad, India: Vide Leaf, 2022. https://videleaf.com/wp-content/uploads/2022/02/Prime-Archives-in-Material-Science_4th-Edition.png.
29. Kurmaz, S.V., Fadeeva, N.V., Skripets, J.A., Komendant, R.I., Ignatiev, V.M., Emel'yanova, N.S., Soldatova, Y.V., Faingold, I.I., Poletaeva D.A., and Kotel-

nikova, R.A., New water-soluble forms of a-tocopherol: preparation and study of antioxidant activity *in vitro, Mendeleev Commun.*, 2022, vol. 32, p. 117. https://doi.org/10.1016/j.mencom.2022.01.038

30. Kurmaz, S.V., Ignatiev, V.M., Emel'yanova, N.S., Kurmaz, V.A., Konev, D.V., Balakina, A.A., and Terentyev, A.A., New nanosize systems Doxorubicin—amphiphilic copolymers of *N*-vinylpyrrolidone with (di)methacrylates with antitumor activity, *Pharmaceutics*, 2022, vol. 14, p. 2572. https://doi.org/10.3390/pharmaceutics14122572
31. Kurmaz, S.V., Ivanova, I.I., Fadeeva, N.V., Perepelitsina, E.O., Lapshina, M.A., Balakina, A.A., and Terent'ev, A.A., New amphiphilic branched copolymers of *N*-vinylpyrrolidone with methacrylic acid for biomedical applications, *Polym. Sci. A*, 2022, vol. 64, p. 434. https://doi.org/10.1134/S0965545X22700237
32. Kurmaz, S.V., Ivanova, I.I., Emelyanova, N.S., Konev, D.V., Kurmaz, V.A., Filatova, N.V., Balakina, A.A., and Terentiev, A.A., Doxorubicin compositions with biocompatible terpolymer of *N*-vinylpyrrolidone, methacrylic acid and triethylene glycol dimethacrylate, *Mendeleev Commun.*, 2023, vol. 33, p. 255. https://doi.org/10.1016/j.mencom.2023.02.034
33. Konev, D.V., Lizgina, K.V., Istakova, O.I., Baulin, V.E., Kalashnikova, I.P., Devillers, C.H., and Vorotyntsev, M.A., Electropolymerization of magnesium 5, 15-di(*N*-methoxyphenyl) porphine, *Russ. J. Electrochem.,* 2016, vol. 52, p. 1150. https://doi.org/10.1134/S1023193516120077
34. Sakhapov, I.F., Gafurov, Z.N., Babaev, V.M., Kurmaz, V.A., Mukhametbareev, R.R., Rizvanov, I.Kh., Sinyashin, O.G., and Yakhvarov, D.G., Electrochemical properties and reactivity of organonickel sigma complex [NiBr(Mes)(bpy)] (Mes = 2,4,6-Trimethylphenyl, bpy = 2,2'-Bipyridyl), *Russ. J. Electrochem.*, 2015, vol. 51, p. 1061. https://doi.org/10.1134/S1023193515110142
35. Oliveira-Brett, A.M., Vivan, M., Fernandes, I.R., and Piedade, J.A.P., Electrochemical detection of in situ adriamycin oxidative damage to DNA, *Talanta*, 2002, vol. 56, p. 959. https://doi.org/10.1016/S0039-9140(01)00656-7
36. Frisch, M.J., Trucks, G.W., Schlegel, H.B., Scuseria, G.E., Robb, M.A., Cheeseman, J.R., Scalmani, G., Barone, V., Mennucci, B., Petersson, G.A., et al., *Gaussian 09, Revision, B.01*; Gaussian Inc.: Wallingford, CT, USA, 2009.
37. Laikov, D.N., Fast evaluation of density functional exchange-correlation terms using the expansion of the electron density in auxiliary basis sets, *Chem. Phys. Lett.*, 1997, vol. 281, p. 151. https://doi.org/10.1016/S0009-2614(97)01206-2
38. Tao, J.M., Perdew, J.P., Staroverov, V.N., and Scuseria, G.E., Climbing the density functional ladder: Nonempirical meta-generalized gradient approximation designed for molecules and solids, *Phys. Rev. Lett.*, 2003, vol. 91, p. 146401. https://doi.org/10.1103/PhysRevLett.91.146401
39. Espinosa, E., Molins, E., and Lecomte, C., Hydrogen bond strengths revealed by topological analyses of experimentally observed electron densities, *Chem. Phys. Lett.,* 1998, vol. 285, p. 170. https://doi.org/10.1016/S0009-2614(98)00036-0
40. Tomilov, A.P., Mairanovsky, S.G., Fioshin, M.Ya., and Smirnov, V.A., *Elektrokhimiya organicheskikh soedinenii* (Electrochemistry of Organic Compounds), Leningrad: Khimiya, 1968.
41. Mairanovsky, S.G., Stradyn', J.P., and Bezuglyi, V.D., *Polyarografiya v organicheskoi khimii* (Polarography in Organic Chemistry), Moscow: Khimiya, 1975.
42. Hammerich, O., Oxidation of oxygen-containing compounds, in*: Organic Electrochemistry. An Introduction and a Guide, Baizer, M.M. and Lund, H.*, Eds, New York: Marcel Dekker, 1983, p.1093.
43. Krayz, G.T., Bittner, S., Dhiman, A., and Becker, J.Y., Electrochemistry of quinones with respect to their role in biomedical chemistry, *Chem. Rec.*, 2021, vol. 21, p. 2332. https://doi.org/10.1002/tcr.202100069
44. Rusakov, A.I., Mendkovich, A.S., Gultyai, V.P., and Orlov, V.Yu., *Struktura i reaktsionnaya sposobnost' organicheskikh anion-radikalov*, (Structure and Reactivity of Organic Anion Radicals), Moscow: Mir, 2005.
45. Krivenko, A.G., Kotkin, A.S., and Kurmaz, V.A., The beta-hydroxyethyl radical as a model system for two-pathway electroreduction in the presence of proton donors, *Mendeleev Commun.*, 1998, vol. 8, p. 56. https://doi.org/1070/MC1998v008n02ABEH000922
46. Krivenko, A.G., Kotkin, A.S., and Kurmaz, V.A., Mechanism of electroreduction of intermediates with and without a proton donor, *Electrochim. Acta*, 2002, vol. 47, p. 3891. https://doi.org/10.1016/S0013-4686(02)00358-4
47. Kurmaz, V.A. and Gultyai, V.P., Electrode reactions and electroanalysis of organomercury compounds, *Russ. Chem. Rev.*, 2010, vol. 79, p. 307. https://doi.org/10.1070/RC2010v079n04ABEH004062
48. Baldwin, R.P., Packett, D., and Woodcock, T.M., Electrochemical-behavior of adriamycin at carbon paste electrodes, *Anal. Chem.*, 1981, vol. 53, p. 540. https://doi.org/10.1021/ac00226a037
49. Rao, G.M., Lown, J.W., and Plambeck, J.A., Electrochemical studies of anti-tumor antibiotics. 3. Daunorubicin and Adriamycin, *J. Electrochem. Soc.*, 1978, vol. 125, p. 534. https://doi.org/10.1149/1.2131493
50. Berg, H., Horn, G., Luthardt, U., and Ihn, W., Interaction of anthracycline antibiotics with bio-polymers. 5. Polarographic-behavior and complexes with DNA, *Bioelectrochem. Bioenergetics*, 1981, vol. 8, p. 537. https://doi.org/10.1016/0302-4598(81)80025-6
51. Kano, K., Konse, T., Nishimura, N., and Kubota, T., Electrochemical properties of adriamycin adsorbed on a mercury-electrode surface, *Bull. Chem. Soc. Jpn.*, 1984, vol. 57, p. 2383. https://doi.org/10.1246/bcsj.57.2383
52. Kano, K., Konse, T., and Kubota, T., The effects of the pH and the temperature on the oxidation-reduction properties of adriamycin adsorbed on a mercury-electrode surface, *Bull. Chem. Soc. Jpn.*, 1985, vol. 58, p. 424. https://doi.org/10.1246/bcsj.58.424

53. Kano, K., Konse, T., Hasegawa, K., Uno, B., and Kubota, T., Electrochemical study of the mechanism and kinetics of reductive glycoside elimination of adriamycin adsorbed on a mercury-electrode surface, *J. Electroanalyt. Chem.*, 1987, vol. 225, p. 187. https://doi.org/10.1016/0022-0728(87)80013-X

54. Kano, K., Konse, T., and Kubota, T., The curve fitting analysis of DC and AC voltammograms of a 2-step surface-redox reaction—the application to the surface-redox system of adriamycin adsorbed on a pyrolytic-graphite electrode, *Bull. Chem. Soc. Jpn.*, 1985, vol. 58, p. 1879. https://doi.org/10.1246/bcsj.58.1879

55. Konse, T., Kano, K., and Kubota, T., Determination of the equilibrium and kinetic-parameters for the surface-redox reaction of hydroquinone moiety of adsorbed adriamycin by means of numerical-simulation of DC voltammogram, *Bull. Chem. Soc. Jpn.*, 1986, vol. 59, p. 265. https://doi.org/10.1246/bcsj.59.265

56. Komorsky-Lovric, S., Redox kinetics of adriamycin adsorbed on the surface of graphite and mercury electrodes, *Bioelectrochem.*, 2006, vol. 69, p. 82. https://doi.org/10.1016/j.bioelechem.2005.10.006

57. Komorsky-Lovric, S. and Lovric, M., Electrode reaction of adriamycin interpreted as two consecutive electron transfers with stabilization of the intermediate, *Coll. Czechosl. Chem. Commun.*, 2007, vol. 72, p. 1398. https://doi.org/10.1135/cccc20071398

58. Vacek, J., Havran, L., and Fojta, M., The reduction of doxorubicin at a mercury electrode and monitoring its interaction with DNA using constant current chronopotentiometry, *Collect. Czech. Chem. Commun.*, 2009, vol. 74, p. 1727. https://doi.org/10.1135/cccc2009512

59. Nieciecka, D. and Krysinski, P., Interactions of doxorubicin wectith self-assembled monolayer-modified electrodes: Electrochemical, surface plasmon resonance (SPR), and gravimetric studies, *Langmuir*, 2011, vol. 27, p. 1100. https://doi.org/10.1021/la103583g

60. Hahn, Y.H. and Lee, H.Y., Electrochemical behavior and square wave voltammetric determination of doxorubicin hydrochloride, *Arch. Pharm. Res.*, 2004, vol. 27, p. 31. https://doi.org/10.1007/BF02980041

61. Oliveira-Brett, A.M., Piedade, J.A.P., and Chiorcea, A.M., Anodic voltammetry and AFM imaging of picomoles of adriamycin adsorbed onto carbon surfaces, *J. Electroanal. Chem.*, 2002, vol. 538–539, p. 267. https://doi.org/10.1016/S0022-0728(02)00944-0

62. Malatesta, V., Penco, S., Sacchi, N., Valentini, L., Vigevani, A., and Arcamone, F., Electrochemical deglycosidation of anthracyclines—stereoelectronic requirements, *Can. J. Chem.,* 1984, vol. 62, p. 2845. https://doi.org/10.1139/v84-481

63. Ozalp-Yaman, S., Onal, A.M., and Turker, L., Electrochemical and quantum chemical studies on mitomycin and adriamycin, *J. Mol. Struct.*, 2003, vol. 654, p. 81. https://doi.org/10.1016/S0022-2860(03)00176-5

64. Land, E.J., Mukherjee, T., Swallow, A.J., and Bruce, J.M., One-electron reduction of adriamycin: Properties of the semiquinone, *Arch. Biochem. Biophys.*, 1983, vol. 225, p. 116. https://doi.org/10.1016/0003-9861(83)90013-9

65. Vajdle, O., Zbiljic, J., Tasic, B., Jovic, D., Guzsvany, V., and Djordjevic, A., Voltammetric behavior of doxorubicin at a renewable silver-amalgam film electrode and its determination in human urine, *Electrochim. Acta*, 2014, vol. 132, p. 49. https://doi.org/10.1016/j.electacta.2014.03.124

66. Golabi, S.M. and Nematollahi, D., Polarographic-determination of doxorubicin and daunorubicin in pharmaceutical preparations and biological media, *J. Pharm. Biomed. Anal.*, 1992, vol. 10, p. 1053. https://doi.org/10.1016/0731-7085(91)80118-S

67. Jemelkova, Z., Zima, J., and Barek, J., Voltammetric and amperometric determination of doxorubicin using carbon paste electrodes, *Collect. Czech. Chem. Commun.*, 2009, vol. 74, p. 1503. https://doi.org/10.1135/cccc2009081

68. Vacek, J., Havran, L., and Fojta, M., Ex situ voltammetry and chronopotentiometry of doxorubicin at a pyrolytic graphite electrode: redox and catalytic properties and analytical applications, *Electroanalysis*, 2009, vol. 21, p. 2139. https://doi.org/10.1002/elan.200904646

69. Haghshenas, E., Madrakian, T., and Afkhami, A., Electrochemically oxidized multiwalled carbon nanotube/glassy carbon electrode as a probe for simultaneous determination of dopamine and doxorubicin in biological samples, *Anal. Bioanal. Chem.*, 2016, vol. 408, p. 2577. https://doi.org/10.1007/s00216-016-9361-y

70. Skalova, S., Langmaier, J., Barek, J., Vyskocil, V., and Navratil, T., Doxorubicin determination using two novel voltammetric approaches: A comparative study, *Electrochim. Acta*, 2020, vol. 330, 135180. https://doi.org/10.1016/j.electacta.2019.135180

71. Hajian, R., Shams, N., and Mohagheghian, M., Study on the interaction between Doxorubicin and deoxyribonucleic acid with the use of methylene blue as a probe, *J. Braz. Chem. Soc.*, 2009, vol. 20, p. 1399. https://doi.org/10.1590/S0103-50532009000800003

72. Chaney, E.N. and Baldwin, R.P., Voltammetric determination of doxorubicin in urine by adsorptive preconcentration and flow-injection analysis, *Anal. Chim. Acta*, 1985, vol. 176, p. 105. https://doi.org/10.1016/S0003-2670(00)81637-2

73. Chaney, E.N. and Baldwin, R.P., Electrochemical determination of adriamycin compounds in urine by preconcentration at carbon paste electrodes, *Anal. Chem.*, 1982, vol. 54, p. 2556. https://doi.org/10.1021/ac00251a034

74. Wang, M.F., Lin, J., Gong, J.W., Ma, M.C., Tang, H.L., Liu, J.Y., Yan, F., and Yan, F., Rapid and sensitive determination of doxorubicin in human whole blood by vertically-ordered mesoporous silica film modified electrochemically pretreated glassy carbon electrodes, *RSC Adv.*, 2021, vol. 11, p. 9021. https://doi.org/10.1039/d0ra10000e

75. Brzozowska, M. and Krysinski, P., Synthesis and functionalization of magnetic nanoparticles with covalently bound electroactive compound doxorubicin, *Electrochim. Acta*, 2009, vol. 54, p. 5065. https://doi.org/10.1016/j.electacta.2008.11.018

76. Fülöp, Z., Gref, R., and Loftsson, T., A permeation method for detection of self-aggregation of doxorubicinin aqueous environment, *Int. J. Pharm.,* 2013, vol. 454, p. 559. https://doi.org/10.1016/j.ijpharm.2013.06.058

77. Yanylkin, V.V. and Krivenko, A.G., *Elektrokhimiya nanosistem* (Electrochemistry of Nanosystems), Moscow, RAS, 2021.

78. Lovrich, M., Square-wave voltammetry, in *Electroanalytical Methods. Guide to Experiments and Applications*, Scholz, F., Ed., Berlin: Springer, 2002, p. 121.

79. Laviron, E., General expression of the linear potential sweep voltammogram in the case of diffusionless electrochemical systems, *J. Electroanal. Chem.*, 1979, vol. 101, p. 19. https://doi.org/10.1016/S0022-0728(79)80075-3

80. Kurmaz, S.V., Fadeeva, N.V., Ignat'ev, V.M., Kurmaz, V.A., Kurochkin, S.A., and Emel'yanova, N.S., Structure and state of water in branched *N*-vinylpyrrolidone copolymers as carriers of a hydrophilic biologically active compound, *Molecules*, 2020, vol. 25, p. 6015. https://doi.org/10.3390/molecules25246015

81. Demin, A.M., Vakhrushev, A.V., Valova, M.S., Korolyova, M.A., Uimin, M.A., Minin, A.S., Chistyakov, K.A., Krasnov, V.P., and Charushin, V.N., Features of doxorubicin adsorption on Fe_3O_4 magnetic nanoparticles coated with SiO_2 or SiO_2/aminopropylsilane, *Mendeleev Commun.*, 2023, vol. 33, p. 160. https://doi.org/10.1016/j.mencom.2023.02.004

82. Kuwabara, T., Noda, T., Ohtake, H., Ohtake, T., Toyama, S., and Ikariyama, Y., Classification of DNA-binding mode of antitumor and antiviral agents by the electrochemiluminescence of ruthenium complex, *Anal. Biochem.*, 2003, vol. 314, p. 30. https://doi.org/10.1016/S0003-2697(02)00651-6

Translated by T. Safonova